Regular Article

PHYSICAL CHEMISTRY RESEARCH
Published by the
Iranian Chemical Society
www.physchemres.org
info@physchemres.org

Phys. Chem. Res., Vol. 8, No. 4, 719-735, December 2020
DOI: 10.22036/pcr.2020.217921.1727

Computational Study of the Precursor Spectroelectrochemistry of Guanine

F. Tabesh and H. Sabzyan*
Department of Chemistry, University of Isfahan, Isfahan 81746-73441, I. R. Iran
(Received 30 January 2020, Accepted 13 July 2020)

Precursor spectroelectrochemical behavior of guanine is investigated based on UV-Vis absorption and fluorescence, and IR and Raman spectra of guanine and its radical cation in the presence of a model electrode, computed using (TD)M06/6-31++G** method. Effects of electrode potential (V_E^e), molecule-electrode distance (d) and molecular orientations (θ) on this behavior are investigated. Results indicate that application of electric potential causes changes in the molecular structure and distribution of charge and spin densities, which consequently changes the electronic and vibrational characteristics of the system. Also, perturbation due to the applied electric potential, changes both the intensities and frequencies of the vibrational bands of the studied species. The absorption wavelength, and the peak intensity and width of the electronic spectra of guanine and its radical cation also show sensitivity to the applied electrode potential. Presence of solvent both as electrostatic medium and as explicit solvent (molecules) have significant effects on the spectroelectrochemical properties of guanine, and change the chemical activity of guanine radical cation formed by the electrode reaction. Furthermore, population and orbital analyses show that for all orientations, application of the electric potential by the electrode increases contribution of the inter-molecular (guanine→water) charge density displacement to the UV-Vis transitions.

Keywords: Spectroelectrochemistry, DFT-M06/6-31++G**, UV-Vis, Fluorescence, IR and raman spectra, Guanine, Radical cation

INTTRODUCTION

Spectroelectrochemical (SEC) method, as a combination of spectroscopic and electrochemical techniques, is used to investigate simultaneously the kinetics, thermodynamics, and molecular details of surface phenomena, including electrochemical reactions at the electrode-electrolyte interfaces. The SEC studies can thus provide better and deeper understanding of the structure of matter and the mechanism of electrochemical reactions, as compared to the individual compilation of the electrochemical and spectroscopic studies. So far, many experimental SEC studies have been carried out using different spectroscopic (UV-Vis, laser, Raman, IR, NMR and ESR/EPR) and electrochemical (CV, SWV and chronocoulometry) techniques, each requires its own special setup and cell [1,2]. The UV-Vis and Raman spectroscopies are the most widely used SEC methods [3-7]. All these SEC methods have been applied in the investigations on solar cells [8], fuel cells [9] and fiber optic sensors [10], in addition to more standard applications in electrochemistry [11], surface chemistry [12] and corrosion [13]. Despite numerous experimental research works appeared in the literature [14,15], only a limited number of theoretical [16,17] and quantum computational [18,19] descriptive studies have been reported on the SEC processes and phenomena. Therefore, developing appropriate computational approach for the detailed study of SEC phenomena at molecular and atomic scales is of great importance. For this purpose, a well-studied and benchmark chemical system, for which experimental spectroscopic, electrochemical and SEC data are available, is a prerequisite.

In the present computational study, the precursor SEC behavior of guanine and its radical cation (Fig. 1) is investigated using density functional theory quantum computation method, and a simple molecular modeling for

*Corresponding author. E-mail: sabzyan@sci.ui.ac.ir

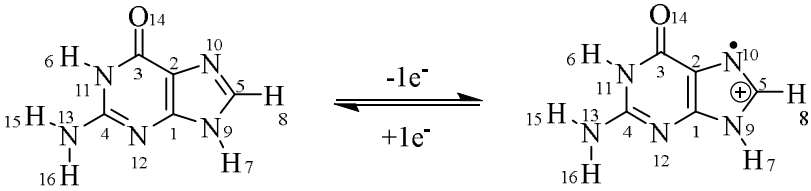

Fig. 1. Radical cation formation in the first step of guanine oxidation [20].

the electrode surface and application of electric potential. Success of this method in obtaining information on changes in the electronic and vibrational spectra of the studied species, under applied electrode potential, is also demonstrated. This research is designed and carried out to obtain molecular insight and understanding from the precursor phenomena occurring just prior to the electrochemical reaction of the aimed molecule, not accessible via routine experimental electrochemical studies. Upon availability of adequate computational facilities, our method can be extended to the electrochemical reactions also using full quantum mechanical modeling of the electrode and electrochemical reactions.

Guanine consisting of a fused pyrimidine-imidazole conjugated ring system, is one of the five nucleobases found in DNA and RNA, and thus is an important molecular system in organic, biochemistry and physical chemistry. So far, a number of experimental and computational spectroscopic characterization and electrochemical studies have been carried out on guanine [20-30]. Also, several experimental SEC studies have been performed on guanine. For example, oxidation mechanism of guanine is studied by surface-enhanced Raman scattering SEC method [31]. In addition to the determination of the vibrational frequencies of guanine and the intermediates resulting from its oxidation, variations in the orientation of these species on the surface of gold nanoparticles during the electrochemical oxidation are also studied in this work. The use of EPR-SEC method for the study of guanine radical formation is also reported [32]. Also, an UV-Vis-SEC monitoring technique is used to follow electrocatalytic oxidation of guanine on the $[Ru(bpy)_2(MPyTMPP)Cl]^+$/ITO electrode [33].

COMPUTATIONAL PROCEDURES

The reaction model used in this computational study is as follows:

$$M + E \longrightarrow M^+ \cdots e^- + E \longrightarrow M^+ \cdots e^- \cdots E \longrightarrow M^+ + e^- \cdots E \longrightarrow M^+ + E^-$$

In this model, M (M^+), E and e^- denote respectively the molecule (its radical cation), electrode and transferring electron. In order to investigate the effect of electrode potential on structural and bonding characteristics and spectroelectrochemical (SEC) behavior of the guanine (G), guanine-electrode (G-E), guanine-solvent-electrode (G-S-E), guanine radical cation ($G^{\bullet+}$), guanine radical cation-electrode ($G^{\bullet+}$-E) and guanine radical cation-solvent-electrode ($G^{\bullet+}$-S-E), their structures are optimized at density functional theory (DFT) level with M06 functional and 6-31++G** basis set (*i.e.* M06/6-31++G** method) using G09 program [34]. Variations of the structural, electronic and electrical properties of these species in various applied potentials are analyzed to discover response of their spectral properties to the applied electrochemical potential. Electronic (UV-Vis absorption and fluorescence) and vibrational (IR and Raman) spectra are calculated for these species using time-dependent DFT (TD-DFT) method and harmonic oscillator analysis. These spectra are analyzed to investigate the effect of the electrode potential (V_E^c) and the molecule-electrode distance (d) on the spectral characteristics. Also, effect of molecular orientation with respect to the electrode surface (θ) on the SEC behavior of guanine is investigated.

The most stable tautomer structure of guanine existing in biological systems (Fig. 1) [35] is considered for this study. The model electrode (E) is constructed by aligning $n_{tot} = 45$ model atoms in a $n_x \times n_y = 5 \times 9$ rectangular arrangement having a $d = 3$ Å closest distance (adopted from the Au-Au distance in a gold crystal, 2.88 Å). This electrode

can thus be considered to have a surface area of $A = L_x \times L_y = 405$ Å (with $L_x = n_x d$ and $L_y = n_y d$ being dimensions of the electrode). In order to have the best compatibility with the corresponding real system, a certain electric point charge is allocated to each of these model atoms, as described below.

The G-E ($G^{\bullet+}$-E) and G-S-E ($G^{\bullet+}$-S-E) systems are built and the corresponding appropriate electrode potentials are evaluated according to the following steps.

Evaluation of the Electrode Potential

To allocate an appropriate point charge (q_i) to the model atoms of the model electrode, so that the electrode can apply a potential equal to the standard oxidation potential of guanine, the charge density (σ) of the Au(100) surface measured experimentally at this potential [36] is used. At pH = 7.4 and pH = 13.1, the oxidation potential of guanine at the gold electrode surface versus the Ag/AgCl reference electrode is reported to be +0.69 V [20] and +0.10 V [31], respectively, which are equivalent to V_E^0 = +0.91 V and V_E^0 = +0.32 V referenced to the normal hydrogen electrode (NHE). In this work, calculations are performed for both of these potentials. Basically the following criteria can be considered for selecting appropriate values of the electrode potential. *i*) They should be obtained from experimental oxidation potentials of guanine at the gold electrode surface. *ii*) They should be low enough to avoid induction of electrochemical reaction, and set the molecule just at the precursor stage. *iii*) The surface charge density of the gold electrode at these potential values (needed for our model) be available in the literature. *iv*) At least two electrode potential values sufficiently separated should be available so that the difference in the results can be clearly observable.

The point charge q_i is obtained using the following set of equations.

$$\sigma(C)A = q_{tot}(C) \tag{1}$$

$$V_E^0(C) = \frac{q_{tot}(C)}{C} \tag{2}$$

$$q_i(V_E^0(C) = \frac{q_{tot}(C)}{n_{tot}} \tag{3}$$

In these equations, $q_{tot}(C)$ and σ(C) are the total charge and surface charge density of the electrode at the applied potential of $V_E^0(C)$, and A is its surface area. Also, n_{tot} = 45 is the total number of constituting atoms of the model electrode. Evaluation of the atomic (point) charges of the model electrode is carried out by sequential evaluation of the required quantities starting from the working potential of interest in the order of $V_E^0(C) \rightarrow C \rightarrow \sigma(C) \rightarrow q_{tot}(C) \rightarrow q_i(V_E^0)$. The required data for this sequential evaluation is obtained as follows.

First, the (C, σ(C)) data reported by Panzram *et al.* [36] for the Au(100) gold electrode of A = 1 cm^2 surface area is reproduced in Fig. 2a. Knowing the electrode surface area (A = 1 cm^2), the corresponding total charge $q_{tot}(C)$ values and then the electrode potential $V_E^0(C)$ values are calculated using Eqs. (1) and (2), respectively. The correlation between the capacitance values C and the electrode potential values $V_E^0(C)$, *i.e.* the $C,(V_E^0(C))$ data, is thus obtained for the whole range of the (C, σ(C)) data and plotted in Fig. 2b. Now, at each given electrode potential (*e.g.* $V_E^0(C)$ = +0.32 and +0.91 V, at which electrochemical study is carried out on guanine [31]), the corresponding capacitance value C is obtained using the $C,(V_E^0(C))$ correlation diagram of Fig. 2b, as shown by the vertical and horizontal arrows in this Figure. Then, the surface charge density σ(C) corresponding to the obtained capacitance value C, is obtained using the (C, σ(C)) correlation diagram plotted in Fig. 2a, indeed the corresponding to the given electrode potential $V_E^0(C)$. The charge density obtained in this way, is then used to calculate the $q_{tot}(C)$ values, from which the corresponding atomic (point) charge $q_i(V_E^0(C))$ is calculated using Eq. (3), considering n_{tot} = 45. This procedure resulted in the $q_i(V_E^0(C))$ = +0.0891e and +0.1795e values at the given potentials $V_E^0(C)$ = +0.32 V & 0.91 V, respectively.

It is important to note that experimental values of the surface charge densities at the desired potentials (Fig. 2) are obtained in aqueous 1 M $HClO_4$ solution, which is equivalent to one mole of H^+ per 55 mole of H_2O. To apply this pH in our calculations, at least 55 molecules of water are needed for inclusion of each H^+ species. Due to this limitation, no H^+ ion is included in the present calculations, which results (at least in part) in the differences between

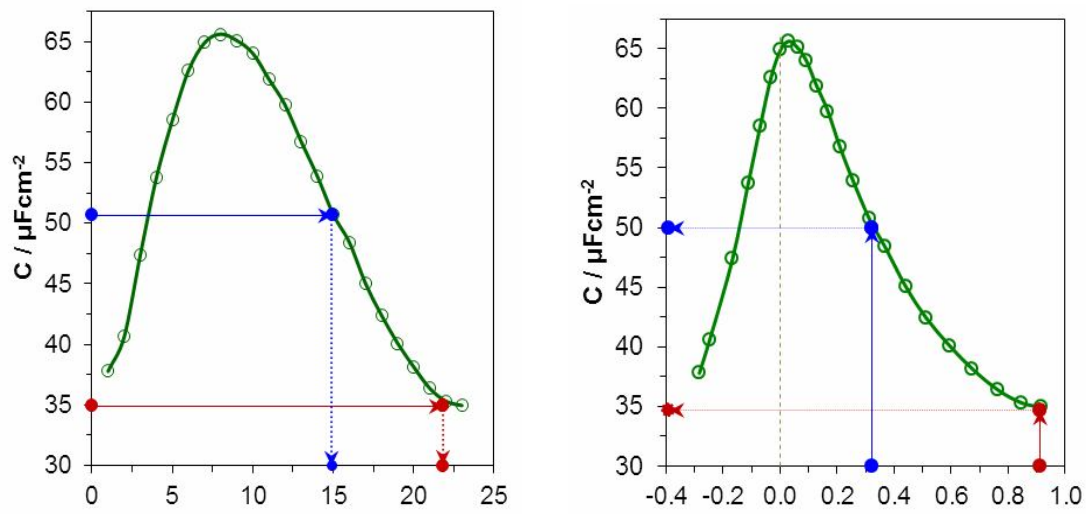

Fig. 2. (a) The (C, σ(C)) data for the Au(100) surface in aqueous 1 M $HClO_4$ re-produced from the data reported by Panzram *et al.* [36]. (b) The $C,(V_E^0(C))$ data derived from the data in (a) using Eqs. (1) and (2) as described in the text.

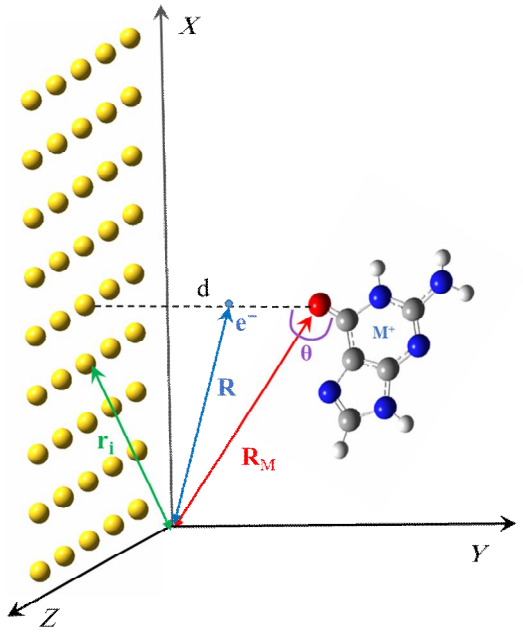

Fig. 3. The setup used in this work to evaluate electric potentials applied on the transferring electron by the guanine molecular core M^+ and the electrode of potential V_E°. The vectors **R**, $\mathbf{R}_M$, and $\mathbf{r}_i$ show the position vectors of the electron, molecule and the model atom number *i*, respectively, and d is the distance of the molecule from the electrode surface.

computational and experimental results.

Setup of the Molecule Position

The setup used in this research to describe the potential applied on the transferring electron is shown in Fig. 3. Appropriate position of the molecule (M) with respect to the surface of the model electrode (E), *i.e.* R_M, at which the electrode potential has significant contribution to the potential of the transferring electron as a prerequisite for the start electrochemical process, is determined based on the potential energy diagram plotted at each electrode potential V_E^0 as shown in Fig. 4. The potential curves plotted in this Figure are obtained as described below.

The total electric potential applied on the transferring electron at each point R on the line connecting vertically the molecule to the surface of the electrode is the sum of the potentials applied by the molecule $V_M(\mathbf{R})$ and the potential applied by the electrode $V_E(\mathbf{R})$, *i.e.*

$$V_{tot}(\mathbf{R}) = V_M(\mathbf{R}) + V_E(\mathbf{R}) \quad (4)$$

In this equation, the molecule and the electrode potentials are given by:

$$V_M(\mathbf{R}) = \frac{1}{4\pi\varepsilon_0}\frac{(-1e)(+q_M e)}{|\mathbf{R}-\mathbf{R}_M|} \quad (5)$$

$$V_E(\mathbf{R}) = \frac{1}{4\pi\varepsilon_0}\sum_i \frac{(-1e)(+q_i e)}{|\mathbf{R}-\mathbf{r}_i|} \quad (6)$$

where e is the charge of electron, q_M is the charge of remaining radical cation after leaving the electron (*i.e.* + 1), $\mathbf{r}_i$ is the position vector of the electrode model atom number i having charge $+q_i e$.

In Fig. 4, the total electric potentials applied on the transferring electron by the molecular core (M^+) and the electrode (E) for different molecular positions (d) calculated for the electrode potentials of V_E^0 = +0.32 and + 0.91 V using Eqs. ((2)-(4)), are shown. The horizontal dashed line in this figure represents the HOMO energy of the isolated guanine (G) which is equal to its ionization potential of the transferring electron, *i.e.* E_{HOMO} = -IP [37]. The curves having maxima above this energy level represent the situation in which ballistic electron transfer is forbidden, and electron transfer can only occur *via* tunneling, while, those having maxima below the HOMO energy level, can undergo ballistic electron transfer and allow electrochemical reaction. At a given potential, at long distances of the molecule from the electrode surface (*i.e.* large d), the transferring electron feels an intermediate plateau potential. Also, it is obvious that at higher electrode potentials, the molecule can be oxidized at farther distances from the electrode surface. It should be noted that the point charges used in this model usually overestimates the electrostatic interaction potential. Therefore, the curves presented in Fig. 4 display the lowest limits of the potentials felt by the transferring electron during the precursor of the electrochemical reaction. In other words, the actual interaction potential felt by the electron is higher than that predicted by our model.

Based on the setup introduced in Fig. 3 and the potential curves presented in Fig. 4 and the above discussion, at each electrode potential, two positions (at 6 and 10 Å distances from the center of the electrode surface) are considered for the molecule. At these distances, the transferring electron will not be ionized, and thus, the electrode reaction is in its precursor stage.

Solvent Structure Models for G-S-E and $G^{\bullet+}$-S-E Systems

To study the effect of solvent on the SEC behavior of G and $G^{\bullet+}$, calculations are performed in aqueous solvent model medium using self-consistent reaction field (SCRF) method and conductor-like polarizable continuum model (CPCM) at each potential and position of the molecule. Also, effect of the explicit solvent molecules on the structural, electronic, electrical and spectral properties of G and $G^{\bullet+}$ are investigated. For this purpose, two solvent configurations, as shown in Fig. 5, are considered for each of the G-S-E and $G^{\bullet+}$-S-E systems. In the first model (M1) 9 water molecules are set around the molecule while it is located at 6 Å distance from the electrode surface. The second model (M2) has one water molecule less than that considered in the M1 model, and the molecule-electrode distance is adjusted to 5.5 Å. These calculations are carried out only for the V_E^0 = +0.32 V electrode potential.

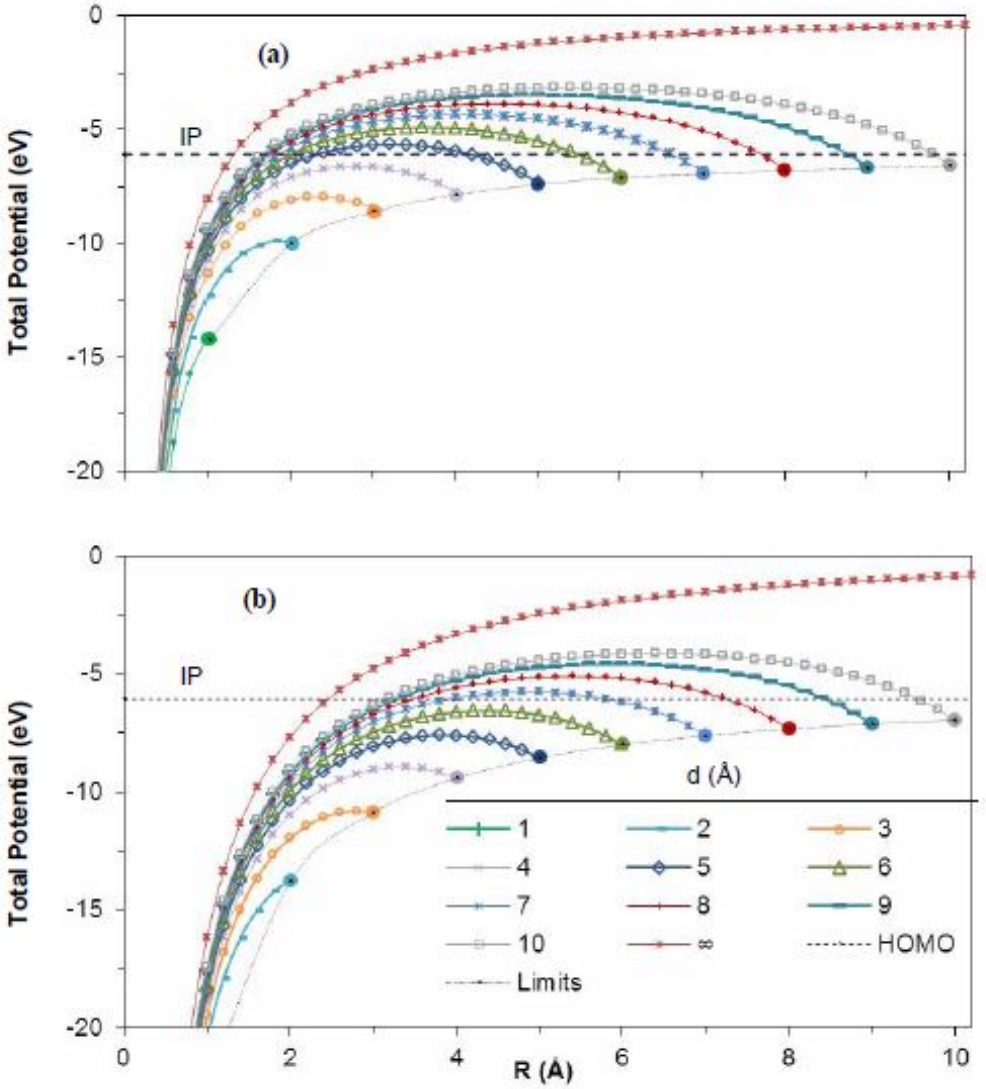

Fig. 4. The potential diagram demonstrating the total electric potential applied on the transferring electron by the molecular core (M^+) and the electrode (E) for different molecular positions (d) calculated at the electrode potentials of (a) V_E° = +0.32 V and (b) V_E° = +0.91 V using Eqs. ((2)-(4)). The large circles show potential of the transferring electron when located on the molecule at the given distance from the electrode surface. The horizontal dashed line represents the HOMO energy of the isolated guanine which is equal to the ionization potential of the transferring electron (*i.e.* the first ionization potential E_{HOMO} = -IP) at zero potential.

Molecular Orientation with Respect to the Electrode Surface

Effect of the molecular orientations on the SEC properties of guanine is investigated by considering five orientations 0, 45, 90, 135 and 180° for the molecule with respect to the electrode surface, defined by the angle θ between the C=O bond and the normal of the electrode surface, as shown in Fig. 3. In this part, the molecule preset at 10 Å distance of the closest atom of guanine from the electrode surface. Also, 9 molecules of water are arranged

around guanine according to the M1 model for G-S-E system. Geometry optimization of these systems are carried out at zero potential and at V_E^c = +0.32 V using the M06/6-31++G**/CPCM method, and their UV-Vis, IR and Raman spectra are then calculated.

RESULTS AND DISCUSSION

Analysis of the Structural, Electronic and Electrical Characteristics

Effects of electrode potential on the characteristics obtained for guanine and its radical cation are presented in the Supplementary Material (Tables S1-S9 and Figs. S1-S4). These characteristics include bond lengths and angles and their variations, atomic charges, spin density distribution, dipole moment, polarizability, frontier orbital shapes and energies and the HOMO-LUMO gap (HLG) which are analyzed below.

Analysis of the structural parameters of guanine reported in Table S1 shows that all bond lengths and angles are affected by the applied potential, but with different scales. The largest variations belong to the C_3=O_{14} & C_3-N_{11}, C_1-C_2 and C_3-C_2 bond lengths in different conditions. Also, variations in the bond angles are very small (with a maximum of 3.4° for the Q_{14}-C_3-N_{11} angle and in the M1 explicit solvent model), and are consequences of the variations in the bond lengths. The molecule remains planar at all conditions with negligible changes in its dihedral angles. Reviewing the data reported in Table S2 for the guanine radical cation, shows that its bond lengths and bond angles are more sensitive to the applied potential and molecule-electrode distance.

The NBO atomic charges calculated for guanine and its radical cation reported in Tables S3 and S4, show that the most positive and negative charges are located on the C_3 and N_{13} atoms, respectively. In most cases, the electric charge of the carbonyl oxygen atom experiences the largest change due to the applied potential because of its non-bonding and pi-bonding electrons and its closest distance to the surface of electrode. At a certain distance of molecule from the electrode surface, increasing the applied potential results in higher negative charges on the atoms located closer to the electrode surface, while at the same time the atoms located farther from the electrode surface acquire more positive charges. It can thus be concluded that the molecule and its radical cation are more polarized along the EF (dipole moment increases) under the applied potential.

The atomic (unpaired electron) spin densities in the guanine radical cation $G^{\bullet+}$ are reported in Table S5. It can be seen from this Table that in the absence of external potential, spin density is distributed mainly over the C_2 > C_5 > N_{12} > N_{13} and O_{14} atoms. Also, spin density over the H_8 atom is largest among all hydrogen atoms, and thus it can better leave the molecule. Furthermore, application of the electric potential changes the electron density distribution so that the main part of the spin density is located on the N_{10}, C_5, C_2 and N_{12} atoms with different orders depending on conditions. Review of the spin densities (Table S5) shows also that the solvation structure affects the distribution of spin density on atoms and, as a result, changes the chemical activity of radical cation formed by the electrode reaction.

The calculated values of the frontier orbital energies for both guanine and its radical cation (Tables S8 and S9) shows decreasing trends with increasing electric potential and decreasing molecule-electrode distance. This decrease is larger for the LUMOs. These orbitals also undergo more significant changes in their shapes shown in Figs. S1-S4.

Spectroscopic and SEC Properties of Guanine and its Radical Cation

Vibrational spectra: IR Spectra: The characteristic band in the vibrational spectra of guanine in the absence of electrode potential (Fig. 6a) belongs to the C_3O_{14} carbonyl stretching mode coupled with the stretching mode of C_2C_3, bending mode of $N_{11}H_6$ and scissoring mode of the NH_2 group, and appear in the range of 1780-1850 cm^{-1} frequencies. This mode, which is labelled as υ_1 in the rest of this report, has been observed experimentally at 1672-1718 cm^{-1} [22,23,31]. In the CPCM medium and in the presence of explicit solvent molecules, the υ_1 band shifts to smaller frequencies and its intensity increases.

In the gas phase and in the CPCM water medium, at a certain distance from the electrode surface, the υ_1 band of guanine is shifted to smaller frequencies with increasing potential, which denote weakening of the C_3-O_{14} bond (Figs. 7a,b and 8a,b). In the case of $G^{\bullet+}$, the same trend is observed (Figs. 7c,d and 8c,d), except for the CPCM water medium at the V_E^0 = +0.32 V and molecule-electrode

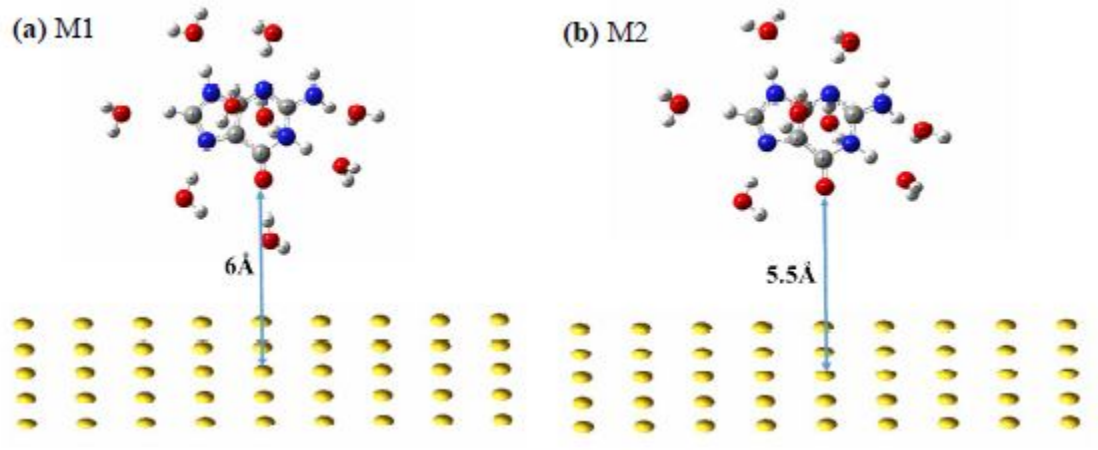

Fig. 5. The explicit solvent configuration models considered for the G-S-E and $G^{\bullet+}$-S-E systems, containing 9 (a) and 8 (b) water molecules around the G or $G^{\bullet+}$ species while located at 6 Å and 5.5 Å, respectively.

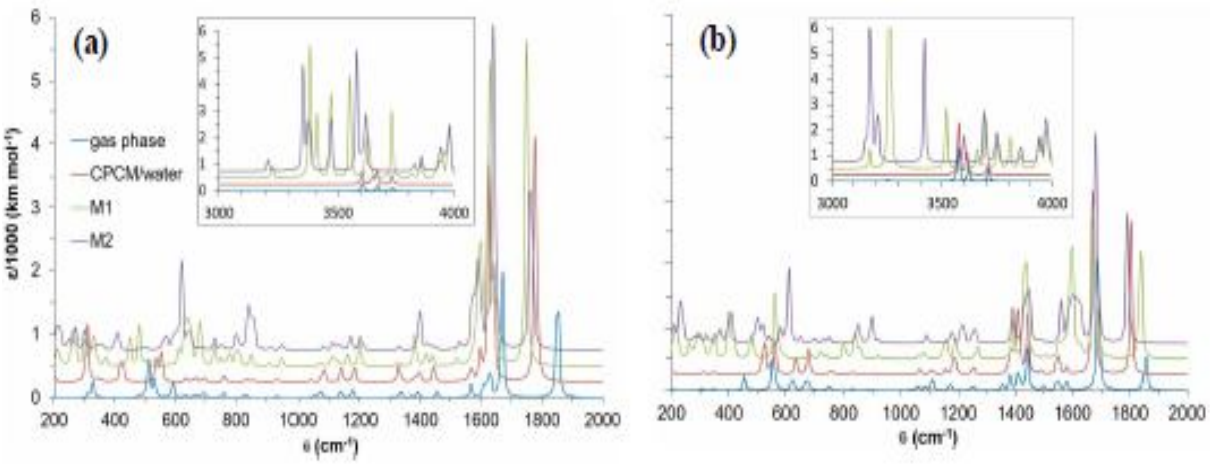

Fig. 6. IR spectra of G (a) and $G^{\bullet+}$ (b) in the absence of electrode potential, for gas phase (blue), CPCM water medium (red), M1 model (green) and M2 model (violet).

distance of d = 10 Å (Fig. 8d). In the M1 model (Fig. 5), increasing potential shifts the υ_1 band of guanine to larger frequencies and reduces its intensity, while in the M2 model, applying potential does not have significant effect on the position and intensity of this band (Figs. S5a and S5b). In the case of $G^{\bullet+}$, by applying the electric potential, υ_1 band is shifted to smaller and larger frequencies in the M1 and M2 models, respectively (Figures S5c and S5d).

Raman spectra: In the Raman spectra of guanine and its radical cation (Figs. S6-S9), the trends of changes due to the application of electric potential are similar to that observed for the IR spectra.

Electronic UV-Vis and fluorescence spectra. *UV-Vis Spectra:* Guanine has an absorption band in the UV region, over the range of 200-300 nm (Fig. 9a). The strong absorption peak (ε = 13000) with a maximum at about 240 nm can be attributed to the existence of a conjugated π system and the non-bonding electron pair of oxygen in the

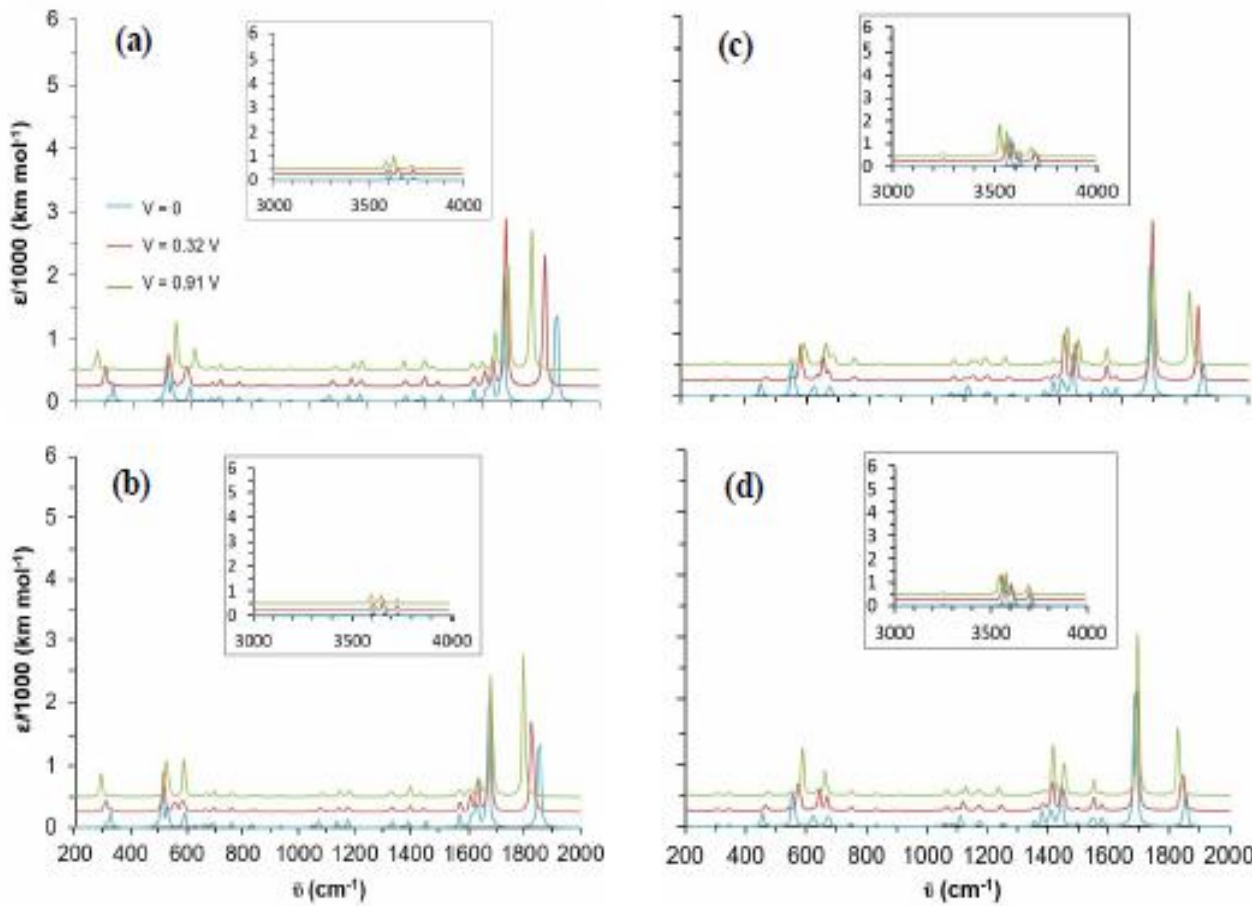

Fig. 7. IR spectra of G and $G^{\bullet+}$ in the gas phase for different applied potentials and different molecular positions: a) G/R = 6 Å, b) G/R= 10 Å, c) $G^{\bullet+}$/R= 6 Å and d) $G^{\bullet+}$/R= 10 Å.

guanine structure. The λ_{max} of guanine has been observed experimentally at about 245 nm [24]. Absorption band of $G^{\bullet+}$ at the UV and beginning of the visible regions in the gas phase (Fig. 9b), has two peaks at 272 nm (related of the electron density displacement from the bridge bond to other parts of the molecule) and 355 nm (related to the electron density displacement from the NH_2, NH and C=O groups towards the bridge region of the molecule). See Table S10 and Fig. S10.

In the gas phase, at a certain distance from the electrode surface, the λ_{max} of guanine shifts to shorter wavelengths with increasing potential (Figs. 10a and 10b). In the case of $G^{\bullet+}$, the peak at 365 nm has a red shift and an increase in its intensity due to the application of electric potential. Also, addition of a weak absorption peak at 218 nm in the UV-Vis spectrum of $G^{\bullet+}$ is a result of the applied potential (Figs. 10c and 10d). In the CPCM water medium (Figs. 11a and 11b), for a specified distance from the electrode surface, application of electric potential shifts the absorption band of guanine to longer wavelengths and decreases its intensity. In particular, at the $V_E^0 = +0.91$ V potential, broadening and reduction in the intensity of the UV-Vis spectrum is very significant. In the M1 and M2 models, application of electric potential shifts the absorption peak of G to longer wavelengths and reduces its intensity (Figs. S11a and S11b). In the case of $G^{\bullet+}$, application of electric potential in the M1 model, increases and decreases intensities of the peak at 362 nm and 458 nm, respectively. While in the M2 model, intensities of both peaks are reduced (Figs. S11c and S11d).

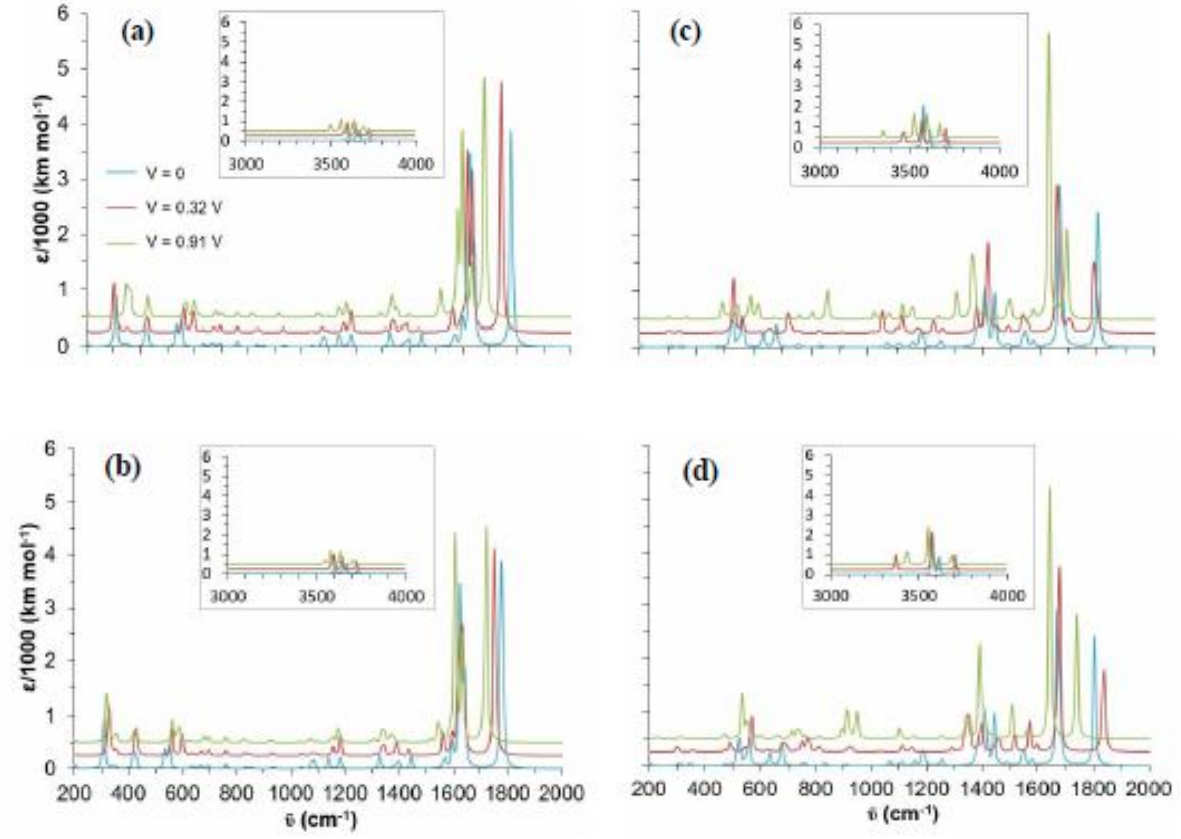

Fig. 8. IR spectra of G and $G^{\bullet+}$ in the CPCM water medium for different applied potentials and different molecular positions: a) G/R = 6 Å, b) G/R = 10 Å, c) $G^{\bullet+}$/R = 6 Å and d) $G^{\bullet+}$/R = 10 Å.

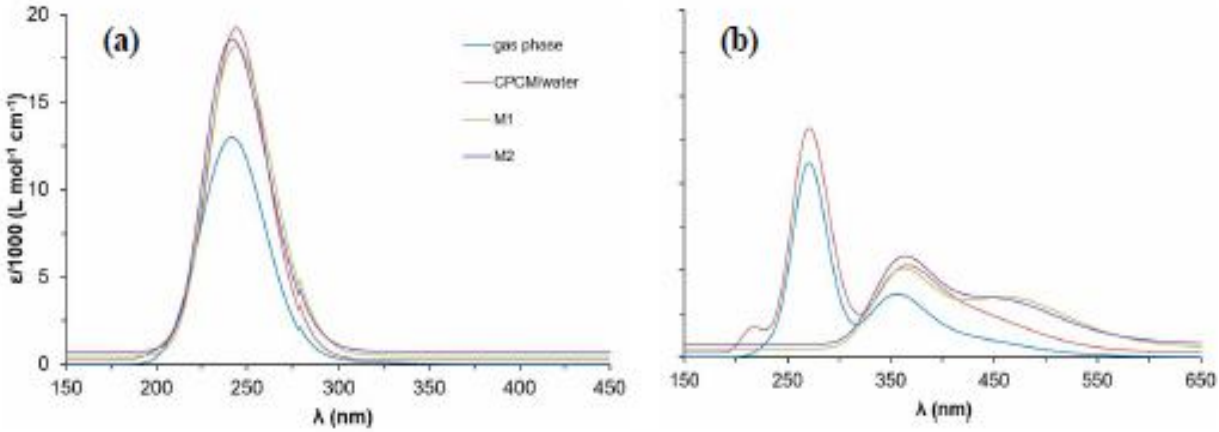

Fig. 9. UV-Vis spectra of G (a) and $G^{\bullet+}$ (b) in the absence of electrode potential, for gas phase (blue), CPCM water medium (red), M1 model (green) and M2 model (violet).

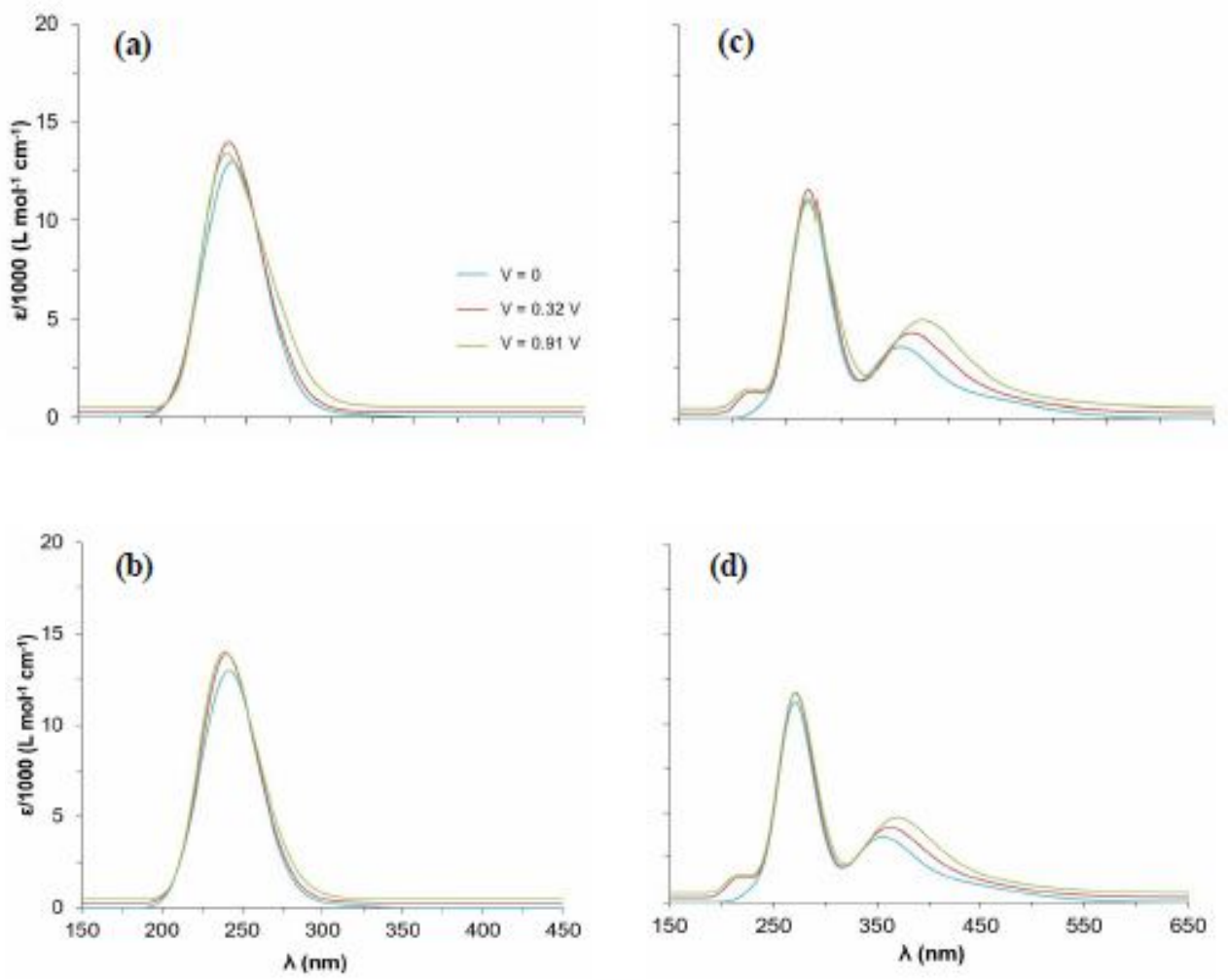

Fig. 10. UV-Vis spectra of G and $G^{\bullet+}$ in the gas phase for different applied potentials and different molecular positions: a) G/R = 6 Å, b) G/R = 10 Å, c) $G^{\bullet+}$/R = 6 Å and d) $G^{\bullet+}$/R = 10 Å.

Fluorescence Spectra: With the optimization of the first excited state, the energy levels of all excited states are improved, and transition dipole moments of these states are corrected. Calculated energies and ground to excited states transition dipole moment components (μ_x, μ_y, μ_z) for the electronic states of guanine and its radical cation in the absence and presence of electric potential are reported in Tables S11 and S12. By applying potential, electronic wavefunctions and their corresponding dipole moment matrix elements change. These changes result consequently in the changes in the arrangement of the polar solvent molecules around the molecule which further affect the electronic states wave functions and energies, and their transition energies. Therefore, it is basically expected that the fluorescence spectra of the neutral and radical cation species G and $G^{\bullet+}$ change when electric field is applied.

Effect of orientation

Geometry of guanine in the G-S-E system is optimized at different initially set orientations (θ_{ini} = 0, 45, 90, 135 and 180°) defined as the angle between the direction of the C=O bond and the normal of the electrode surface as demonstrated in Fig. 3, in the absence and presence of the electric potential of +0.32 V. Vibrational analysis carried

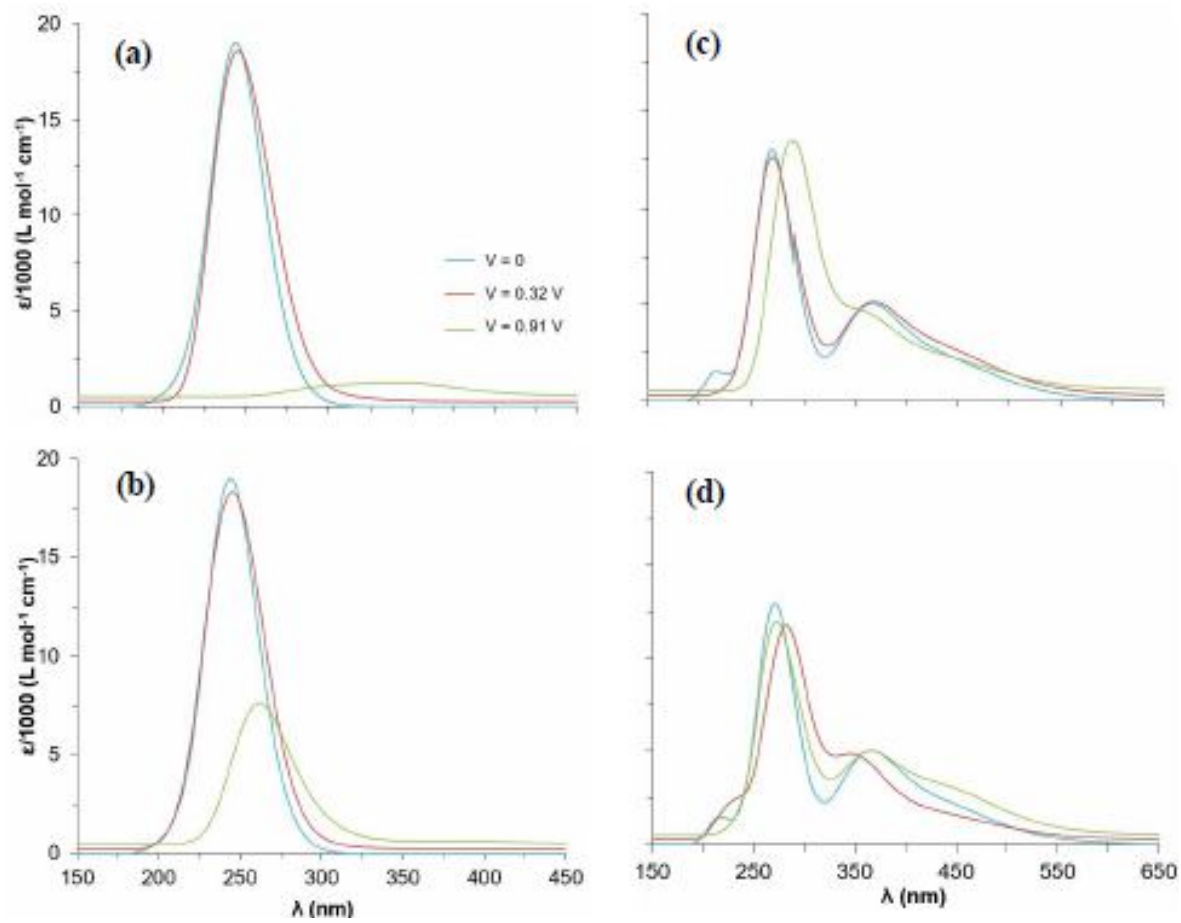

Fig. 11. UV-Vis spectra of G and $G^{\bullet+}$ in the CPCM water medium for different applied potentials and different molecular positions: a) G/R = 6 Å, b) G/R = 10 Å, c) $G^{\bullet+}$/R = 6 Å and d) $G^{\bullet+}$/R = 10 Å.

out to confirm quality of these geometry optimizations, resulted in negative modes with imaginary frequencies smaller than 240*i* cm^{-1} corresponding to the local rotational motions of water molecules having usually low-curvature potential energy surfaces such that location of their minima in these geometry optimization procedure are difficult, and thus the optimized structures are acceptable. Results of these optimizations are presented in Table S13 (a, b, c and d) of the Supplementary Materials. Analysis of these structural data and comparison with those obtained at the reference (perpendicular, θ = 180°) orientation shows that orientation of guanine with respect to the electrode surface has significant effects on its optimized geometry. For example, the optimized orientation (θ_{opt}) of the molecule with respect to the electrode surface, changes from the corresponding initially set values (θ_{ini}) by 5.0-11.5 and 2.8-14.1 degrees in the absence and presence of electric potential applied on the system (See Table 1).

Electrical properties μ_x, μ_y, μ_z, $|\vec{\mu}|$, α_{xx}, α_{yy}, α_{zz} and α_{iso} calculated for the optimized structures in these orientations are reported in Table S13c. A review of these data shows that values of dipole moment $|\vec{\mu}|$ and its components μ_x, μ_y, μ_z in the absence of electric potential varies with the orientation of the molecule which can be attributed to the changes in the arrangement and orientations of water molecules solvating the guanine molecule. Application of electric potential to the electrode, significantly increases the

Table 1. Variations of the Optimized Orientation θ_{opt} in Degrees, Dipole Moment $|\vec{\mu}|$ in Debye, Maximum Absorption Wavelength λ_{max} in nm and the Corresponding Peak Intensity $\varepsilon(\lambda_{max})$ in $M^{-1}cm^{-1}$ with Initially Set Orientation θ_{ini} of the Guanine Molecule Near the Surface of a Gold Electrode under Electric Potential of +0.32 V Obtained by M06/6-311++G** DFT Computations. The Differential Values, Showing the Electric Potential Effect are Given in Parentheses

	θ_{ini}	0	45	90	135	180
$V^{\circ}_E = 0$	θ_{opt}	7.3	50	97	130	168.5
	$\lvert\vec{\mu}\rvert$	12.611	12.399	13.809	11.152	12.064
	λ_{max}	241.7	241.7	241.7	241.7	242.6
	$\varepsilon(\lambda_{max})$	16256.6	16153.4	15197.0	15551.4	16835.9
$V^{\circ}_E = +0.32$ V	θ_{opt}	12.6	52.8	99.3	132.2	165.9
	$\lvert\vec{\mu}\rvert$	16.480	12.241	16.683	11.252	11.732
	$(\Delta\lvert\vec{\mu}\rvert)$	(3.869)	(-0.158)	(2.874)	(0.100)	(0.332)
	λ_{max}	241.7	242	241.7	240.8	244
	$(\Delta\lambda_{max})$	(0.0)	(0.3)	(0.0)	(-0.9)	(-1.4)
	ε_{max}	16806.7	14410.7	14780.2	15056.3	16386.2
	$(\Delta\varepsilon_{max})$	(550.1)	(-1742.6)	(-416.8)	(-495.1)	(449.7)

$|\vec{\mu}|$ for orientations $\theta = 0$ and 90°, while slightly changes the $|\vec{\mu}|$ for other orientations. It can also be seen from this table that application of the external potential does not alter components of the polarizability tensor significantly, regardless of the orientation of the molecule.

The UV-Vis and IR spectra for guanine in different orientations are calculated and plotted in Figure 12. The corresponding maximum absorption wavelengths and intensities are listed in Table 1. The calculated Raman spectra are also presented in Fig. S12 of the Supplementary Materials.

It can be seen in Fig. 12a and Table 1 that at all orientations, the λ_{max} of the UV-Vis absorption spectra of guanine is not significantly shifted with application of electric potential. Also, by applying potential, the peak intensity is decreased for orientations $\theta = 45$, 90 and 135°, and increased for orientations $\theta = 0$ and 180°.

Population and orbital analyses used to determine contributions of the solute (guanine) and solvent (water) atomic orbitals in each UV-Vis transitions for the $\theta = 0$, 90 and 180° orientations, show that these UV-Vis transitions correspond to the charge density displacements of combined intra-molecular and inter-molecular (solute→solvent) natures. Also, contributions of each of these two types of displacements are identical for orientations $\theta = 0$ and 90° (see Table S14 and Fig. S13 and S14). In addition, contribution of the inter-molecular charge density displacement is larger for the orientation $\theta = 180°$, as compared to those for the other two orientations. These population and orbital analyses (Table S14 and Fig. S13 and S14), show furthermore that contribution of the inter-molecular (guanine→water) charge density displacement increases upon application of the electric field potential for

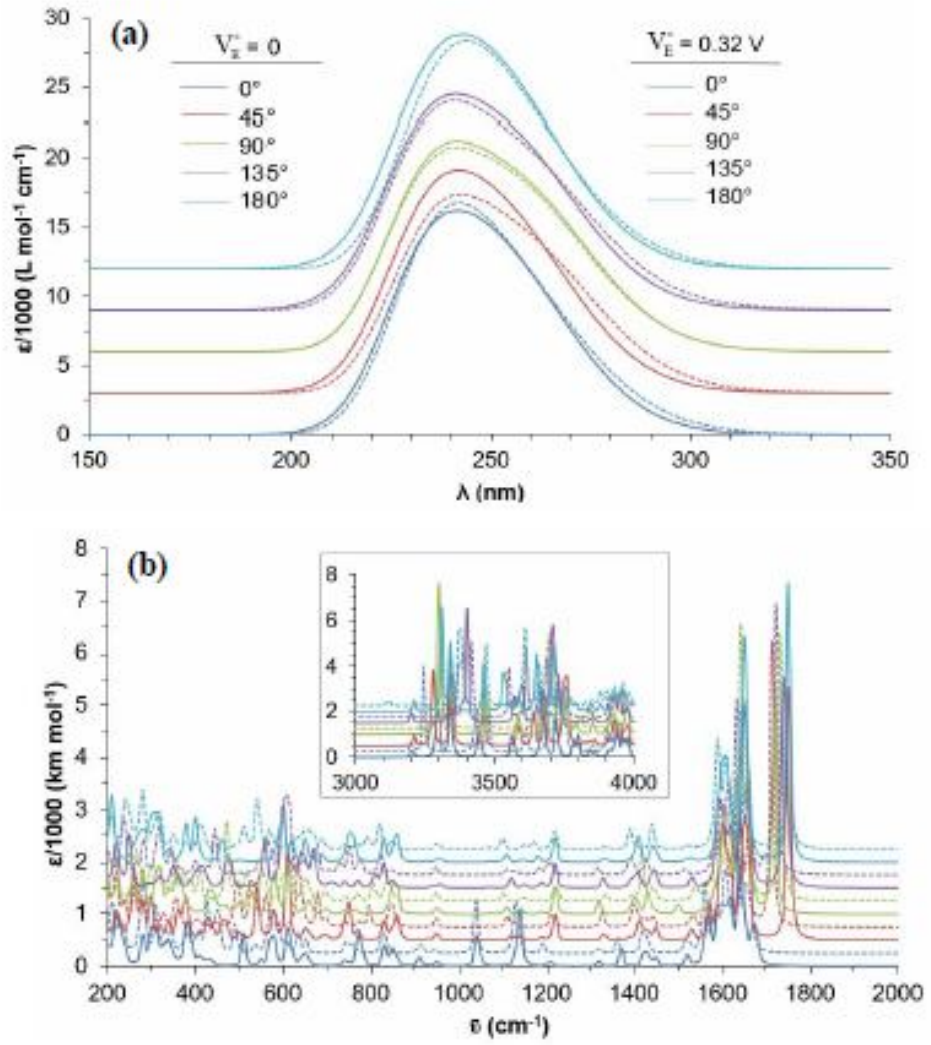

Fig. 12. The TD-M06/6-31++G** calculated UV-Vis (a) and IR (b) spectra of guanine in different orientations (θ = 0, 45, 90, 135 and 180°) with respect to the electrode surface, in the absence of electric potential and at V_E^0 = +0.32 V.

all orientations. Since, solute-solvent partial charge separation results in a stronger interaction, it can be predicted that the excited state guanine is stabilized further by this extra interaction between the solute (guanine) and solvent (water) molecules, and thus the adiabatic transitions in the excited state of the solvated guanine occur at longer wavelengths. It is therefore expected that the fluorescence emission of solvated guanine in this potential appear at longer wavelengths as compared to that in the absence of the electric potential.

In the IR spectra of guanine (Fig. 12b), the υ_1 band (Sec. 3.2.1) is located over the range of 1718-1751 cm^{-1} frequencies, while at orientation θ = 0° this mode appears in 1642 cm^{-1}, which denotes weakening of the C_3-O_{14} bond. With application of electric potential, the υ_1 band is shifted to smaller frequencies, except at the orientation θ = 90°. Intensity of this mode increases by applying electric potential.

CONCLUSIONS

The precursor spectroelectrochemical (SEC) behavior of guanine (G) and its radical cation ($G^{\bullet+}$) are studied by appropriate combination of ab initio density functional theory M06/6-31++G** computations and a simple molecular modeling. Responses of structural, electronic and electrical properties of these two species to electrode potentials of different strengths (V_E^0 = +0.32 and +0.91 V) are analyzed. Effects of electrode potential and molecule-electrode distance on the IR, Raman, UV-Vis and fluorescence spectra of G and $G^{\bullet+}$ in different conditions (gas phase, CPCM water medium and in the presence of explicit solvent molecules) are investigated. Application of electrode potential causes changes in the molecular structure and distribution of charge and spin densities, which consequently changes the electronic and vibrational characteristics of these systems. Analysis of the calculated spectra of the $G/G^{\bullet+}$ species showed that electric potential and distance from the electrode surface change observably both the positions and intensities of the absorption peaks, especially for $G^{\bullet+}$. In addition, it is shown for guanine that molecular orientation with respect to the electrode surface has small, but observable, effect on the SEC properties. At extreme (*i.e.* very long) molecule-electrode distances, the roles of the electrode model, the applied potential and the molecular orientation all become negligible and do not have significant effect on the molecular characteristics. Increasing electrode potential and decreasing molecule-electrode distance have obviously similar effects as both increase the effect of the electric field on the molecule. Molecular orientation has small but observable effect on the spectroelectrochemical properties of the precursor state of guanine which depend on the coordination sphere of the solvent molecules. However, it can be expected that in the electron-transfer step (electrochemical process), the orientation of the molecule should be critical and determining.

Also, population and orbital analyses show that contribution of the inter-molecular (guanine→water) charge density displacement to the UV-Vis transitions increases upon application of the electrode potential for all orientations of the molecule.

REFERENCES

[1] Pletcher, D.; Greff, R.; Peat, R.; Peter, L. M.; Robinson, J., Instrumental Methods in Electrochemistry. Ellis Horwood, 1985, p. 317-355.

[2] León, L.; Mozo, J. D., Designing spectroelectrochemical cells: A review. *TrAC-Trends Anal. Chem.* **2018**, *102*, 147-169, DOI: 10.1016/j.trac.2018.02.002.

[3] Chen, W.; Liu, X. Y.; Qian, C.; Song, X. N.; Li, W. W.; Yu, H. Q., An UV-Vis spectroelectrochemical approach for rapid detection of phenazines and exploration of their redox characteristics, *Biosens. Bioelectron.* **2015**, *64*, 25-29, DOI: 10.1016/j.bios.2014.08.032.

[4] Hernández, C. N.; García, M. B. G.; Santos, D. H.; Heras, M. A.; Colina, A.; Fanjul-Bolado, P., Aqueous UV-Vis spectroelectrochemical study of the voltammetric reduction of graphene oxide on screen-printed carbon electrodes, *Electrochem. Commun.* **2016**, *64*, 65-68, DOI: 10.1016/j.elecom.2016.01.017.

[5] Kalbac, M.; Farhat, H.; Kong, J.; Janda, P.; Kavan, L.; Dresselhaus, M. S., Raman spectroscopy and in situ Raman spectroelectrochemistry of bilayer 12C/13C graphene, *Nano Lett.* **2011**, *11*, 1957-1963, DOI: 10.1021/nl2001956.

[6] Joya, K. S.; Sala, X., *In situ* Raman and surface-enhanced Raman spectroscopy on working electrodes: spectroelectrochemical characterization of water oxidation electrocatalysts, *Phys. Chem. Chem. Phys.* **2015**, *17*, 21094-21103, DOI: 10.1039/C4CP05053C.

[7] Ibañez, D., Garoz-Ruiz, J., Heras, A. and Colina, A., Simultaneous UV-Vis absorption and Raman spectroelectrochemistry, *Anal. Chem.* **2016**, *88*, 8210-8217, DOI: 10.1021/acs.analchem.6b02008.

[8] Kämper, S; Paretzki, A.; Fiedler, J.; Záliš, S.; Kaim, W., Solar cell sensitizer models $[Ru(bpy\text{-}R)_2(NCS)_2]$ probed by spectroelectrochemistry, *Inorg. Chem.* **2012**, *51*, 2097-2104, DOI: 10.1021/ic201825h.

[9] Hagen, A.; Traulsen, M. L.; Kiebach, W. R.; Johansen, B. S., Spectroelectrochemical cell for *in situ* studies of solid oxide fuel cells, *J. Synchrotron Rad.* **2012**, *19*,400-407, DOI: 10.1107/S0909049512006760.

[10] Imai, K.; Okazaki, T.; Hata, N.; Taguchi, S.; Sugawara, K.; Kuramitz, H., Simultaneous multiselective spectroelectrochemical fiber-optic sensor: demonstration of the concept using methylene blue and ferrocyanide, *Anal. Chem.* **2015**, *87*, 2375-2382, DOI: 10.1021/ac504321u.

[11] Bonifas, A. P.; McCreery, R. L., Solid state spectroelectrochemistry of redox reactions in polypyrrole/oxide molecular heterojunctions, *Anal. Chem.* **2012**, *84*, 2459-2465, DOI: 10.1021/ac2032047.

[12] Lotti, D.; Hamm, P.; Kraack, J. P., Surface-sensitive spectro-electrochemistry using ultrafast 2D ATR IR spectroscopy, *J. Phys. Chem. C.* **2016**, *120*, 2883-2892, DOI: 10.1021/acs.jpcc.6b00395.

[13] Adriaens, A.; Dowsett, M., The coordinated use of synchrotron spectroelectrochemistry for corrosion studies on heritage metals, *Acc. Chem. Res.* **2010**, *43*, 927-935, DOI: 10.1021/ar900269f.

[14] Zhai, Y.; Zhu, Z.; Zhou, S.; Zhu, C.; Dong, S., Recent advances in spectroelectrochemistry, *Nanoscale.* **2018**, *10*, 3089-3111, DOI: 10.1039/C7NR07803J.

[15] Dunsch, L., Recent advances in in situ multi-spectroelectrochemistry. *J Solid State Electr.* **2011**, *15*, 1631-1646, DOI: 10.1007/s10008-011-1453-1.

[16] Uziel, Z., Theory of spectroelectrochemistry under galvanostatic conditions − I. Reversible simple charge transfer reaction, *Electrochimica Acta.* **1987**, *32*, 489-495, DOI: 10.1016/0013-4686(87)85019-3.

[17] Xie, Y.; Dong, S., Theory of analytical spectroelectrochemistry: Catalytic process. *J. Electroanal. Chem. Interfacial Electrochem.* **1990**, *291*, 1-10, DOI: 10.1016/0022-0728(90)87172-G.

[18] Prezhdo, O. V.; Boszczyk, W.; Zubkova, V. V.; Prezhdo, V. V., Solute-solvent interactions determine the effect of external electric field on the intensity of molecular absorption spectra, *J. Phys. Chem. A.* **2008**, *112*, 13263-13266, DOI: 10.1021/jp807857m.

[19] Cheuquepán, W.; Pérez, J. M.; Orts, J. M.; Rodes, A., Spectroelectrochemical and DFT study of thiourea adsorption on gold electrodes in acid media, *J. Phys. Chem. C.* **2014**, *118*, 19070-19084, DOI: 10.1021/jp503694m.

[20] Ferapontova, E., Electrochemistry of guanine and 8-oxoguanine at gold electrodes, *Electrochim. Acta.* **2004**, *49*, 1751-1759, DOI: 10.1016/j.electacta.2003.12.006.

[21] Parker, A. W.; Lin, C. Y.; George, M. W.; Towrie, M.; Kuimova, M. K., Infrared characterization of the guanine radical cation: Finger printing DNA damage, *J. Phys. Chem. B.* **2010**, *114*, 3660-3667, DOI: 10.1021/jp9106958.

[22] Lopes, R. P.; Marques, M. P. M.; Valero, R.; Tomkinson, J.; de Carvalho, L. A., Guanine: a combined study using vibrational spectroscopy and theoretical methods, *J. Spectrosc.* **2012**, *27*, 273-292, DOI: 10.1155/2012/168286.

[23] Giese, B.; McNaughton, D., Density functional theoretical (DFT) and surface-enhanced Raman spectroscopic study of guanine and its alkylated derivatives, Part 1. DFT calculations on neutral, protonated and deprotonated guanine, *Phys. Chem. Chem. Phys.* **2002**, *4*, 5161-5170, DOI: 10.1039/B203829C.

[24] Mishra, P. C., Vibrational structures and intensity distributions in the electronic absorption spectra of nucleic acid bases: evidence for non-planarity of guanine. *J. Mol. Struct.* **1986**, *144*, 309-317, DOI: 10.1016/0022-2860(86)85009-8.

[25] Naumov, S.; von Sonntag, C., Guanine-derived radicals: dielectric constant-dependent stability and UV/Vis spectral properties: a DFT study, *Radiat. Res.* **2008**, *169*, 364-372, DOI: 10.1667/RR1082.1.

[26] Randviir, E. P.; Banks, C. E., Electrochemical measurement of the DNA bases adenine and guanine at surfactant-free graphene modified electrodes, *RSC Adv.* **2012**, *2*, 5800-5805, DOI: 10.1039/C2RA20173A.

[27] Yin, H.; Zhou, Y.; Ma, Q.; Ai, S.; Ju, P.; Zhu, L.; Lu, L., Electrochemical oxidation behavior of guanine and adenine on grapheme-nafion composite film modified glassy carbon electrode and the simultaneous determination, *Process Biochem.* **2010**, *45*, 1707-1712, DOI: 10.1016/j.procbio.2010.07.004.

[28] Barman, K.; Jasimuddin, S., Electrochemical detection of adenine and guanine using a self-assembled copper(II)-thiophenyl-azo-imidazole complex monolayer modified gold electrode, *RSC*

Adv. **2014**, *4*, 49819-49826, DOI: 10.1039/C4RA08568J.

[29] Oliveira-Brett, A. M.; Diculescu, V.; Piedade, J. A. P., Electrochemical oxidation mechanism of guanine and adenine using a glassy carbon microelectrode, *Bioelechem.* **2002**, *55*, 61-6, DOI: 10.1016/S1567-5394(01)00147-5.

[30] Psciuk, B. T.; Schlegel, H. B., Computational prediction of one-electron reduction potentials and acid dissociation constants for guanine oxidation intermediates and products, *J. Phys. Chem. B.* **2013**, *117*, 9518-9531, DOI: 10.1021/jp4062412.

[31] Ibañez, D.; Santidrian, A.; Heras, A.; Kalbáč, M.; Colina, A., Study of adenine and guanine oxidation mechanism by surface-enhanced Raman spectroelectrochemistry, *J. Phys. Chem. C.* **2015**, *119*, 8191-8198, DOI: 10.1021/acs.jpcc.5b00938.

[32] Ribaut, C.; Bordeau, G.; Perio, P.; Reybier, K.; Sartor, V.; Reynes, O.; Fabre, P. L.; Chouini-Lalanne, N., EPR spectroelectrochemical investigation of guanine radical formation and environment effects, *J. Phys. Chem. B.* **2014**, *118*, 2360-2365, DOI: 10.1021/jp500952q.

[33] Wu, J. W.; Mei, W. M. J.; Yan, Z. H.; Liu, J. C.; Li, H., *In situ* spectroelectrochemical monitoring during the electrocatalytic oxidation of guanine on [Ru $(bpy)_2$(MPyTMPP)Cl]$^+$/ITO electrode, *Electroanal. Chem.* **2013**, *697*, 21-27, DOI: 10.1016/j.jelechem.2013.03.013.

[34] Frisch, M. J.; Trucks, G. W.; Schlegel, H. B.; Scuseria, G. E.; Robb, M. A.; Cheeseman, J. R.; Scalmani, G.; Barone, V.; Mennucci, B.; Petersson, G. A.; Nakatsuji, H.; Caricato, M.; Li, X.; Hratchian, H. P.; Izmaylov, A. F.; Bloino, J.; Zheng, G.; Sonnenberg, J. L.; Hada, M.; Ehara, M.; Toyota, K.; Fukuda, R.; Hasegawa, J.; Ishida, M.; Nakajima, T.; Honda, Y.; Kitao, O.; Nakai, H.; Vreven, T.; Montgomery, J. A.; Jr., Peralta, J. E.; Ogliaro, F.; Bearpark, M.; Heyd, J. J.; Brothers, E.; Kudin, K. N.; Staroverov, V. N.; Kobayashi, R.; Normand, J.; Raghavachari, K.; Rendell, A.; Burant, J. C.; Iyengar, S. S.; Tomasi, J.; Cossi, M.; Rega, N.; Millam, J. M.; Klene, M.; Knox, J. E.; Cross, J. B.; Bakken, V.; Adamo, C.; Jaramillo, J.; Gomperts, R.; Stratmann, R. E.; Yazyev, O.; Austin, A. J.; Cammi, R.; Pomelli, C.; Ochterski, J. W.; Martin, R. L.; Morokuma, R.L.; Zakrzewski, V. G.; Voth, G. A.; Salvador, P.; Dannenberg, J. J.; Dapprich, S.; Daniels, A. D.; Farkas, O.; Foresman, J. B.; Ortiz, J. V.; Cioslowski, J.; Fox, D. J. Gaussian 09, Revision A.1, Gaussian, Inc., Wallingford CT, 2009.

[35] Marian, C. M., The guanine tautomer puzzle: quantum chemical investigation of ground and excited states, *J. Phys. Chem. A.* **2007**, *111*, 1545-1553, DOI: 10.1021/jp068620v.

[36] Panzram, E.; Baumgärtel, H.; Roelfs, B.; Schröter, C.; Solomun, T., A capacitance and infrared study of the electrical double layer structure at single crystal gold electrodes in acetonitrile, *Ber. Bunsenges. Phys. Chem.* **1995**, *99*, 827-837, DOI: 10.1002/bbpc.19950990607.

[37] Koopmans, T., Über die zuordnung von wellenfunktionen und Eigenwerten zu den einzelnen elektronen eines atoms, *Physica.* **1934**, *1*, 104-113. DOI: 10.1016/S0031-8914(34)90011-2.